Research Article

Guoyuan Wang*, Wenbo Fan, Qingbin Shi, and Yingqi Luo

Analyzing the compressive performance of lightweight foamcrete and parameter interdependencies using machine intelligence strategies

https://doi.org/10.1515/rams-2025-0126
received January 27, 2025; accepted June 12, 2025

Abstract: As an alternate to regular concrete, foam concrete, also called foamcrete, has several useful applications. It saves money on transportation and production costs as well as dead weight on buildings and foundations, which helps with energy efficiency. Nevertheless, there is still a lack of practical applications, which calls for more research, especially in strength studies, to increase its use in the actual world. For this purpose, the compressive strength (C-S) of foamcrete was assessed using two machine learning algorithms: gene expression programming (GEP) and multi-expression programming (MEP). A sensitivity analysis was conducted to determine how important certain aspects were. For predicting foamcrete's compressive strength, MEP was better than GEP. By comparison, the MEP model had an R_2 value of 0.970, while the GEP models only managed 0.94. This is further supported by the findings of the statistical analysis and the ML models' cross-validation using Taylor's diagram. The sensitivity analysis results indicated that density (28.0%), cement content (11.0%), and age (8.5%) were the three most significant criteria influencing overall strength. The generated models can determine the compressive strength of foamcrete for different input parameter values, hence enhancing its practical uses and saving time and financial resources compared to laboratory testing.

Keywords: compressive strength, foamed concrete, machine learning

*** Corresponding author: Guoyuan Wang,** China Coal Construction Group Co., LTD., Beijing, 102218, China, e-mail: zhongmeiyan2024@163.com

Wenbo Fan: China Coal Construction Group Co., LTD., Beijing, 102218, China

Qingbin Shi, **Yingqi Luo:** 49th Engineering Department, China Coal Construction Co., LTD., Handan, Hebei, 056003, China

1 Introduction

Foamcrete is created by mixing cement, water, and a stable, homogeneous foam that has been treated with the appropriate foaming agent [1–3]. In scholarly circles, this material is known by a variety of names, including cellular lightweight concrete, low-density foam concrete, and lightweight cellular concrete [4–7]. It offers effective ways to tackle diverse obstacles encountered in construction activities. This material has fewer chemicals, aligning with sustainability and environmental requirements, and can occasionally be partially or wholly replaced by conventional concrete [8,9]. It is widely used for thermal insulation [10,11], sound absorption [12,13], and fire resistance [14,15] due to its textural surface and microstructural cells. In recent years, a large number of environmentally conscious buildings have been built using foamcrete for nonstructural purposes [16,17]. To avoid differential settlement, it is used to fill bridge abutments [18]. Also reported are uses for airport buffer systems [19], foundations for buildings [20,21], and the production of prefabricated components [22]. Foam concrete is used in building projects in several nations, including the US, UK, Canada, and Germany [23].

Interest in subsurface engineering has been reignited by this material. Managing the underlying dead load is essential for underground buildings [24–26], and one effective way to do this is by using adjustable density and minimal self-weight [26]. This material's rising popularity is due in large part to its many desirable properties, such as its resilience to earthquakes, its ideal coordinated deformation capacity, and its simplicity of pumping [27,28]. Foam concrete is now making rapid strides as a subsurface project material. Because of its exceptional self-flowing capabilities, it can be used to fill voids, sinkholes, abandoned subways, decommissioned sewage pipelines, and similar situations. It is suitable for use as a linear component in metro and tunnel systems or for load relief because of its small and controlled self-weight [29–31].

Despite the scarcity of studies on the actual applications of foam concrete in civil engineering, its qualities have been adequately investigated. Nonetheless, further investigation of its strength-related properties is vital to broaden its applicability, as strength is a critical characteristic for any material [32–35]. To better understand how foamcrete responds to stress and strain, Fu *et al.* [36] investigated its compression deformation properties when used as a liner element. The results of their experiments showed that while confining pressure and density both increase foamcrete's compressive strength, modulus of elasticity is positively correlated with density alone, regardless of pressure. Contrary to expectations, we found that peak strain increased with confining pressure but showed no significant correlation with density. The freeze–thaw resistance of cellular concrete was studied by Tikalsky *et al.* [37], who proposed a better way to test for this phenomenon. The depth of absorption is a crucial determinant in the formulation of freeze–thaw-resistant concrete, potentially improving the application of foamcrete as an insulating material for tunnels in frigid areas. Sun *et al.* [38] provided important information for material specifications and applications by studying the effects of several foaming agents on foamcrete's compressive strength, workability, and drying shrinkage. Ramamurthy *et al.* [28] classified literature concerning foaming agents, cement, fillers, mix ratios, manufacturing procedures, and the fresh and hardened aspects of foamcrete, whereas Amran *et al.* [27] investigated foamcrete's composition, preparation methods, and attributes. Foamcrete has seen tremendous improvement in its application in the last several decades. In Canada, tunnel grouting with cement-based foamcrete has been widely used [39]. An impact-reducing material for sacrificial tunnel lining cladding was developed by Zhao *et al.* [40] using foam cement. Improved cladding thickness greatly reduced tunnel dynamic reactions to blasting. The effective use of lightweight foamcrete for tunnel drainage in a South Korean dual-lane highway tunnel was credited to the efficient creation and distribution of open-cell foams, which resulted in enhanced permeability, according to Choi and Ma [41]. The essential characteristics of foamcrete remain inadequately examined and require additional research, especially through the utilization of cutting-edge machine learning (ML) methodologies.

The advent of soft computing has allowed for a more accurate representation of many materials' technical characteristics in computer simulations [42,43]. ML models fed data are crucial to the accuracy of predictions [44,45]. It is infamously difficult to precisely estimate construction materials due to their inherent volatility and intricate intricacy. One prominent application of ML techniques in the construction industry is the assessment of engineering properties of materials [46]. The characteristics of both contemporary and classic concrete kinds have been studied using ML methods. This category includes innovative types of concrete such as those enhanced with phase change materials, designed for self-compaction, made lightweight, incorporating recycled aggregates, or reinforced with fibers [47–51]. Strong ML models outperform their more traditional theoretical and experimental equivalents when it comes to estimating certain qualities of concrete engineering, according to multiple study sources. Reliable predictions on the properties of concrete need the resolution of certain computational challenges. Cement hydration and microstructure development are complex processes that present considerable challenges. The activity of cement paste depends on both time and temperature, and this dependency is nonlinear [52–54]. ML algorithms can be trained to accurately anticipate desired features by entering data on combination proportions and curing situations [55]. In addition to being easy to use and requiring low computer power, ML models offer a number of advantages, including generalizability, accuracy, and reproducibility in prediction.

The study suggests that a dependable computational framework for predicting the compressive strength (C-S) of foamcrete could be established using well-trained ML algorithms. This work intends to examine the C-S of foamcrete utilizing robust ML algorithms. Publicly accessible research data was utilized to construct regression models using gene expression programming (GEP) and multi-expression programming (MEP) to forecast the C-S of foamcrete. The dataset comprises a total of 300 points. Mathematical verifications and a Taylor diagram were utilized to confirm the models. In order to determine the extent to which the factors had an impact on the forecast, a sensitivity analysis was carried out. Developing new methods and technologies for automated, low-intervention assessment of material properties has the potential to significantly influence the construction industry as a whole.

2 Methods of research

2.1 Dataset assortment and scrutiny

The creation of effective and widely applicable ML models depends on the availability of accurate and dependable datasets. This study utilizes a dataset of 300 detailed records on compressive strength (C-S), sourced from a previously published article, to investigate the prediction of lightweight foamed concrete strength using GEP and MEP techniques [56].

The experimental data was used to create the model, and it captured the nonlinear correlations between the input variables and concrete strength exceedingly well. There was a deliberate strategy to the data collection process, with an emphasis on including pertinent attributes and using trustworthy sources. The databases utilized nine input factors to build foamcrete: density (Dn), cement (CM), sand (Sa), sand-to-cement ratio (SCR), water-to-cement ratio (WCR), sand size (SS), foaming agent (Ag), foam content (Fm), and age (A). The output variable was C-S. According to previous research, the ideal number of records per input variable for making accurate predictions is at least 5 [57]. The utilization of a dataset of 300 points for C-S, with nine distinct input variables (resulting in 300/9 = 33.33), markedly enhances the observed ratio in this study. The reliability of this database stems from two key factors: (i) the data were generated through experiments carried out in the same laboratory by the same personnel, following uniform international standards and environmental conditions; and (ii) the dataset is sufficiently large to encompass the full range of variables affecting concrete compressive strength. Furthermore, it is a globally recognized resource utilized by other researchers for the advancement of soft computing models, facilitating direct comparisons [58,59].

In building and refining M–L models, the preprocessing of data is an important and vital step. Typical data preprocessing operations encompass handling missing data, encoding, identifying and addressing outliers, and partitioning data [60]. A thorough data pretreatment procedure was implemented to ensure that no outliers were present, even though a multivariate outlier identification technique was not expressly used in the study. Every feature was subjected to univariate outlier identification before the M–L models were trained. Finding and removing data points that did not fall inside the specified acceptable ranges was part of this process. To further ensure that no outliers were missed, the dataset was subjected to extensive statistical and visual analysis. A brief synopsis of the input and output statistical data is provided in Table 1. The statistical measurements provide the ranges of values for the variables, including maximum and minimum. Included as well are the standard deviation, median, kurtosis, skewness, mode, and standard error. The cement content varies from 439.2 to 992.8 kg·m^{-3}, while the density ranges from 1406.91 to 2009.48 kg·m^{-3}. In all C-S situations, the maximum SCR and WCR were maintained at 2.0 and 0.45, respectively. The maximum foam content utilized was 357 kg·m^{-3}, similarly. Additional statistical metrics include data on the mean, variability, kurtosis, and skewness of each input and output. The degree to which the probability distribution of a real-valued variable is asymmetric with regard to its mean is called its skewness. In most cases, an elongated left-hand side of the dispersion curve is indicated when negative numbers are present [61]. The likelihood distribution along the vertical axis can be better understood with the help of kurtosis, a statistical metric that shows if a dataset is appropriate for a specific normal distribution and has light or heavy tails [62].

Additionally, the complete compressive strength (C-S) dataset was randomly divided into two subsets: 70% (210 samples) was used for model training, while the remaining 30% (90 samples) was allocated for validation and testing. For ML model development and evaluation, data must be split into training and test sets. The model parameters are

Table 1: Summary of statistics from the C-S database [63]

Parameters	Density (kg·m^{-3})	Cement (kg·m^{-3})	Sand (kg·m^{-3})	SCR	WCR	Sand-size (mm)	Foaming agent (L)	Foam content (kg·m^{-3})	Age (d)	C-S (MPa)
Mean	1742.771	727.448	733.449	1.06	0.388	0.836	0.176	208.847	17.5	24.845
Standard error	9.89	7.153	8.813	0.022	0.003	0.047	0.011	4.646	0.607	0.655
Median	1758.815	748.55	749.6	1	0.4	0.6	0.2	205	17.5	24.905
Mode	1519.11	770.6	770.6	1	0.45	0.6	0	305	7	18.42
Standard deviation	171.304	123.889	152.652	0.383	0.054	0.822	0.182	80.469	10.518	11.35
Sample variance	29344.97	15348.4	23302.61	0.147	0.003	0.676	0.033	6475.221	110.619	128.824
Kurtosis	−1.061	0.021	0.457	1.975	−1.376	18.016	−1.6	−1.068	−2.013	−0.902
Skewness	−0.22	−0.44	−0.219	1.407	−0.102	4.349	0.28	0.008	0	0.021
Range	602.67	553.6	723.6	1.5	0.15	4.15	0.5	310	21	46.33
Minimum	1406.81	439.2	374.4	0.5	0.3	0.6	0	47	7	2.55
Maximum	2009.48	992.8	1098	2	0.45	4.75	0.5	357	28	48.88
Sum	522831.3	218234.4	220034.8	318	116.4	250.68	52.8	62,654	5,250	7453.46

fitted using the training data, while the model's performance on new data is evaluated objectively using the test set [62]. Avoiding overfitting and getting a good idea of the model's generalizability are both made possible using a separate test set.

The possible impact of input variables on output was also assessed using the Pearson correlation (R) matrix. For C-S, this is graphically shown in Figure 1. R values between −1 and +1 show strong negative or positive connections, while R values close to 0 indicate weak relationships. The inputs exhibit a robust correlation with C-S, evidenced by the maximum positive R-value of 1.0, which clearly substantiates this connection. The proximity of R to zero, indicating a weak correlation, does not always imply that the two variables are entirely independent. This is a significant aspect to consider. Consequently, it is advisable to examine models derived from other studies, such as Shapley Additive exPlanations (SHAP) and sensitivity analysis, to gain a thorough comprehension of the relationship between inputs and outcomes.

The efficiency of the model is strongly correlated with the distribution of the input variables. 3D histogram prism charts, as shown in Figure 2(a)–(i), help to clarify the inputs' proportionate distribution in extensive datasets for C-S. A really random distribution among the polyhedral forms is clearly indicated by the data points. Additionally, noteworthy data clusters, patterns, or outliers can be highlighted by 3D prism charts, allowing for the discovery of trends or possible problems. It is worth noting that the dataset does not contain any clusters or outliers, which suggests that the data points follow a normal distribution. When it comes to ML models, this aspect is paramount.

2.2 ML modeling

To measure foamcrete's compressive strength, a controlled setting was utilized. In order to get the output (C-S), nine inputs were needed. The C-S forecasts for foamcrete were created using cutting-edge ML algorithms like GEP and MEP. In the evaluation of ML algorithms, it is customary to juxtapose the outputs with the input data. Thirty percent of the data was allocated for testing, whereas seventy percent was used to train the ML models. The R^2 value of the predicted outcome indicates the model's effectiveness. R^2 is small for a substantial disparity, indicating that the expected and actual values diverge only marginally [64]. The model's accuracy is corroborated using many approaches, including statistical testing and error assessments. Figure 3 presents a scenario model, while Tables 2 and 3 detail the hyperparameters used for the GEP and MEP models, respectively.

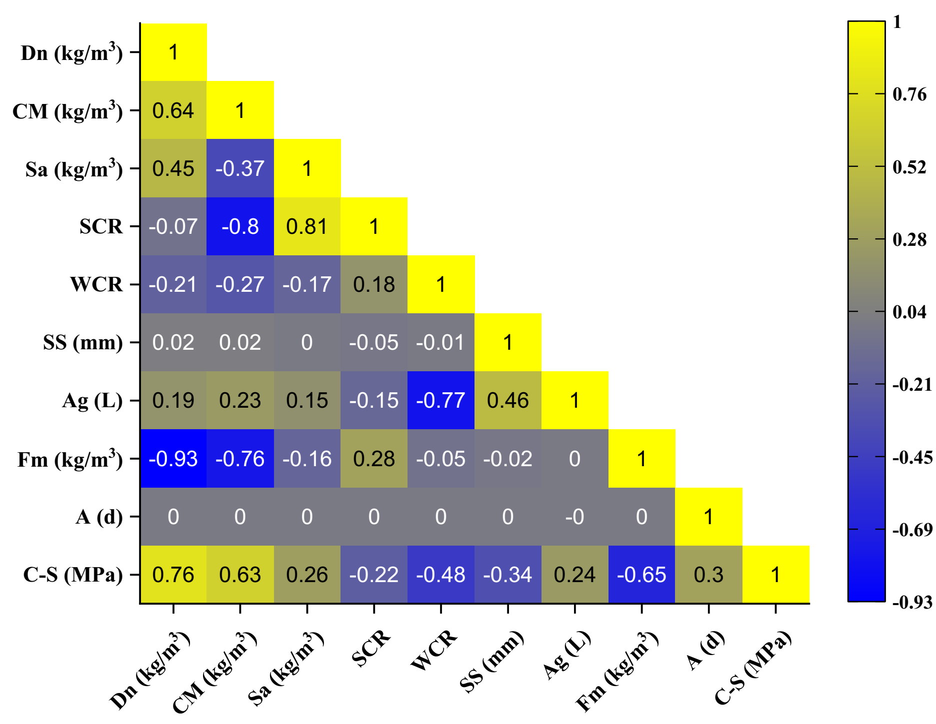

Figure 1: C-S database correlation matrices.

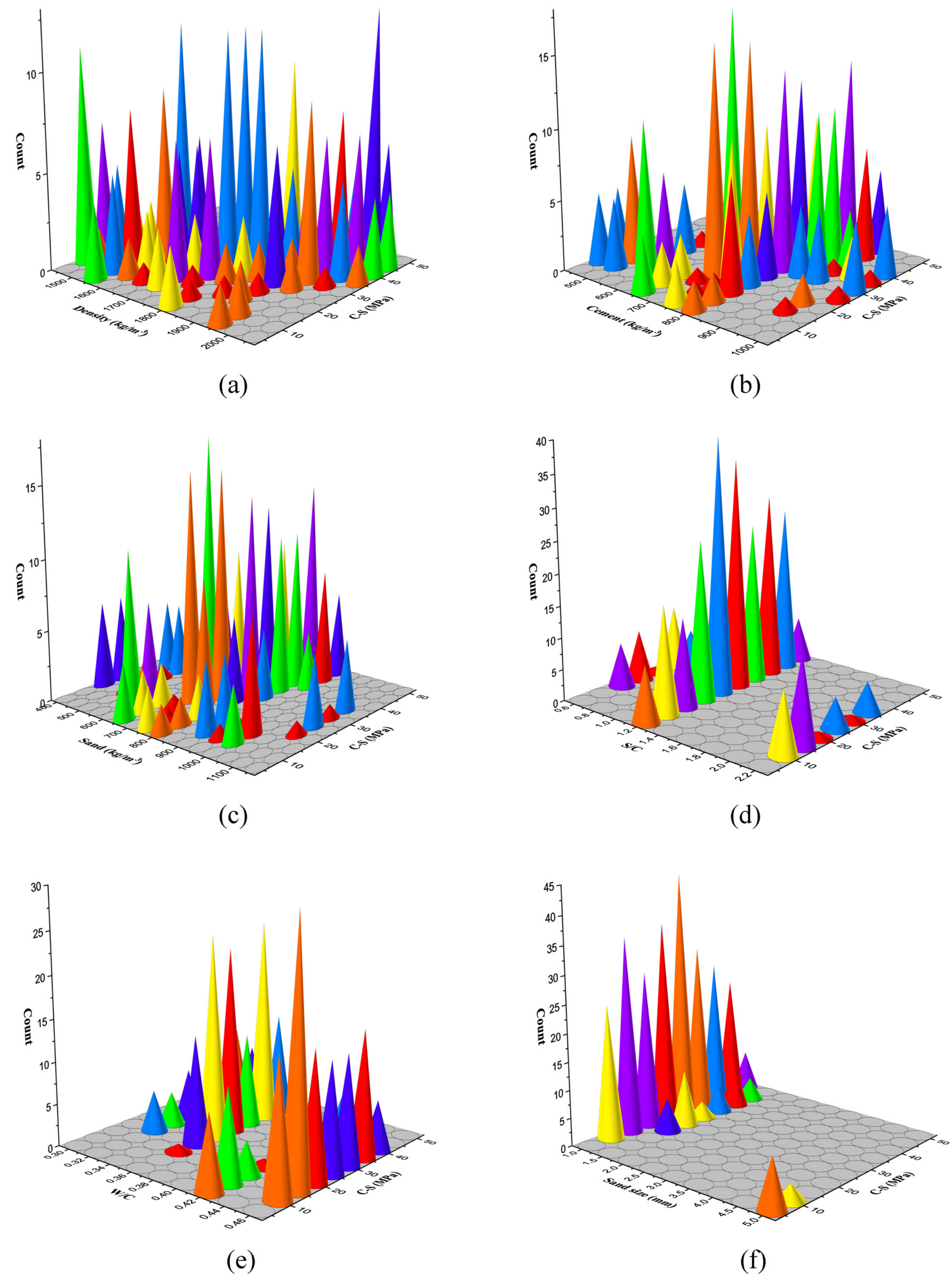

Figure 2: 3D variable frequency histograms for the C-S database: (a) density; (b) cement; (c) sand; (d) S/C; (e) W/C; (f) sand size; (g) foaming agent; (h) foam content; (i) age.

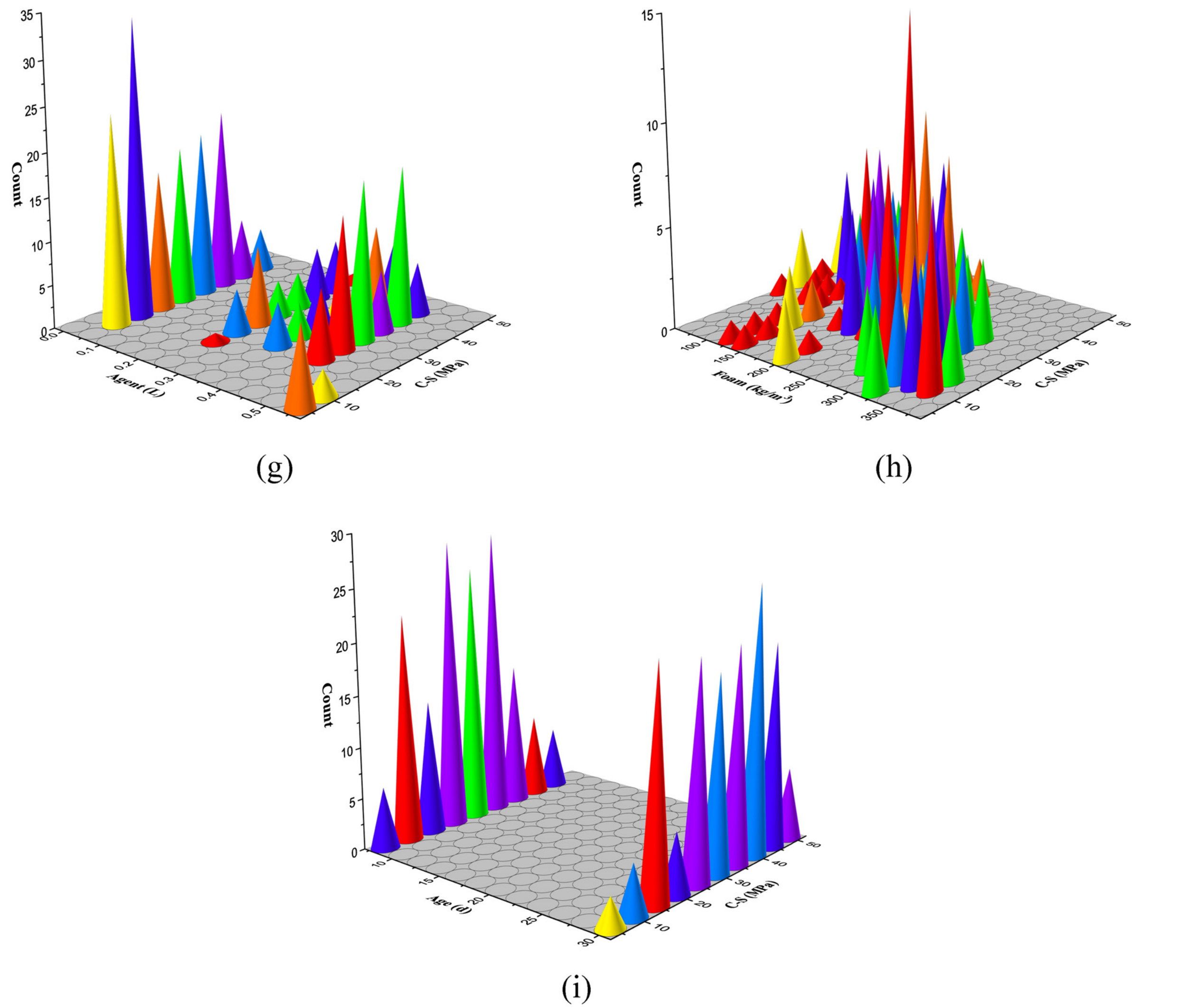

Figure 2: (*Continued*)

2.2.1 GEP ML technique

The genetic algorithm (GA), inspired by Darwin's theory of evolution, was developed by J. H. Holland. In order to address optimization problems, this algorithm mimics the process of natural selection and the principle of survival of the fittest by gradually improving solutions over time [65]. A series of GAs denotes genomic progression, culminating in uniformly sized chromosomes. A novel GA termed "gene programming" was developed by Koza [66]. Genetic programming (GP) employs GAs to create an evolutionary model, serving as a universal approach for problem-solving [67]. In genetic programming, flexibility arises from the ability to utilize nonlinear structures, such as parsing trees, in lieu of fixed-length binary strings. The present artificial neural system aligns with Darwin's theory [68] and utilizes naturally occurring genetic elements (such as procreation, crossovers, and modification) to address reproductive issues. Similar to the last case, the unsuitable trees were removed, and the remaining ones were utilized to replant the area according to our chosen method. However, the evolutionary process helps prevent premature convergence [68,69]. It is essential to ascertain the following five elements prior to using the GP: crucial domain tasks, fitness evaluation, fundamentally useful operators (such population size and crossover), and results from terminals that are specific to the methods used [68]. A crossover genomic processor manages the predominant growth of parse trees, even when the model creation of the GP is reiterated. In nonlinear GP, representations must function as both genotype and phenotype, leading to more complex expressions of desired traits [69].

The original proponent of GP was Candida Ferreira, who was also responsible for inventing GEP. An improvement on classical GP, this method allows for more efficient

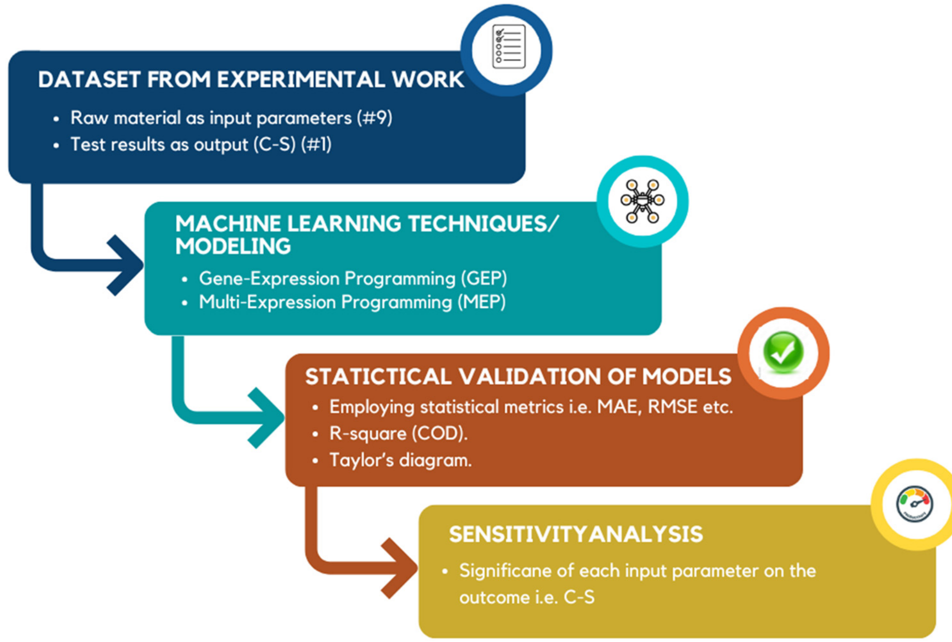

Figure 3: Flow diagram of the approach used from data generation and model validation.

and capable evolution by capturing programs as linear chromosomes and then expressing them as tree topologies [69]. GEP, grounded in the concept of population-based modeling, utilizes linear chromosomes of fixed length and their corresponding parse trees. Often considered an extension of GP, GEP encodes intermediate-sized programs through simple, fixed-length chromosomes. This approach enables the formulation of predictive equations capable of addressing complex and nonlinear problems [70,71]. The termination criteria, final set, and fitness function are all supplied, similar to GP. The "Karva" dialect is used to designate the chromosomes before manufacture, even though the GEP process uses random numbers to generate them. The foundation of GEP is a line with a constant length. In contrast, the data processing of the GP produces parse trees of differing lengths. Individual cords with pronged morphologies of varying diameters depict chromosomes through nonlinear manifestation/parse trees after being defined as genomes of static length [68]. These genotypes and phenotypes can be differentiated by their distinct genetic representations [34]. GEP prevents costly structural modifications and replications by preserving the genome across generations. Because of their unusual "head" and "tail" arrangement, GEP chromosomes are able to generate intricate expressions of several genes from a single copy of DNA. This well-designed structure improves the

Table 2: GEP model standardized factors

Hyper-parameters	Settings	Hyper-parameters	Settings
Genes	4	Stumbling mutation	0.00141
Leaf mutation	0.00546	Constant per gene	10
General	C-S	Inversion rate	0.00546
Head size	10	Gene recombination rate	0.00277
RIS transposition rate	0.00546	Data type	Floating number
		Two-point recombination rate	0.00277
Function set	Addition, subtraction, multiplication, division, square root, and exponential	Chromosomes	250
IS transposition rate	0.00546	Linking function	Addition
Gene transposition rate	0.00277	Lower bound	−10
One-point recombination rate	0.00277	Upper bound	10
Mutation rate	0.00138	Random chromosomes	0.0026

Table 3: MEP model standardized factors

Hyper-parameters	Settings	Hyper-parameters	Settings
Terminal set	Problem input	Error	MSE, MAE
Problem type	Regression	Crossover probability	0.9
Number of generations	250	Number of sub-populations	150
Replication number	15	Sub-population size	100
Mutation probability	0.01	Number of runs	10
Number of treads	2	Function set	Addition, subtraction, multiplication, division, power, square root, and exponential
Operators/variables	0.5	Code length	50

technique's ability to built complex solutions [68]. These genes encode instructions rooted in mathematics, statistics, logic, and Boolean algebra. Activator elements connect these genetic instructions to the specific computational processes they govern, much like how biological DNA regulates cellular functions. Due to the emergence of a novel language named Karva, which is capable of interpreting these chromosomes, equations derived from empirical data are now feasible. An illustrious revolutionary begins their voyage at Karva after the ET. The underneath layer is allocated to nodes by ET utilizing Eq. (1) [70]. It is possible that the total number of ETs is a good predictor of the degree of GEP gene K-expression as well as the duration of that expression

$$\text{ET GEP} = \log\left(i - \frac{3}{j}\right). \tag{1}$$

Unlike less sophisticated ML methods, GEP can learn from data even in the absence of labels. In Figure 4, we can see the numerous steps that go into developing GEP equations. At birth, every cell has the same number of chromosomes. To evaluate everyone's health, these chromosomes must be certified as ETs. Only the fittest and healthiest individuals are able to breed. When the greatest people

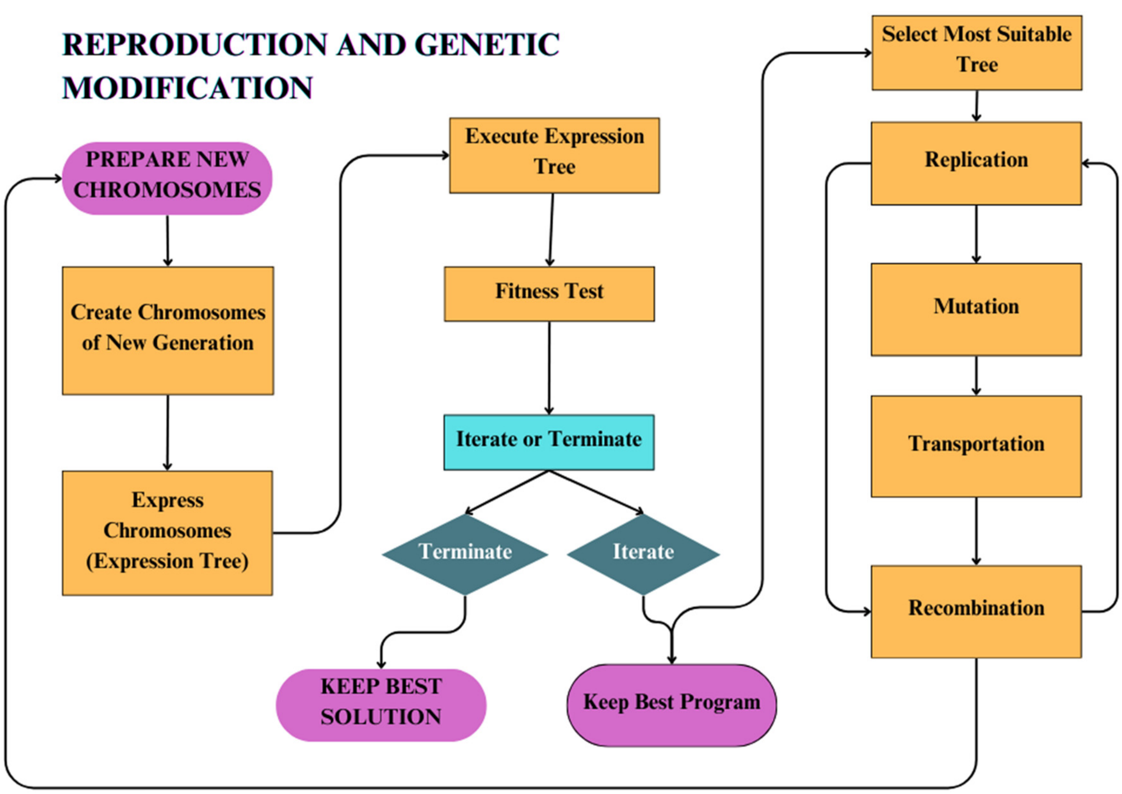

Figure 4: Gene-expression programming workflow diagram [72].

are involved in an iterative process, the outcome is optimal. Following three generations of breeding, mutation, and crossover, the final product is the result of all these operations

2.2.2 MEP ML technique

MEP is considered by some to be a cutting-edge linear variant of GP, distinguished by its use of linear chromosomes. What sets MEP apart from other modern GP approaches is its ability to encode multiple candidate solutions or expressions within a single chromosome. Fitness analysis is employed to choose the most optimum chromosome to accomplish the desired result [73,74]. This occurs when a bipolar system couples twice, leading to the formation of two new generations, as elucidated by Oltean and Grosan. Every generation secures a progenitor for itself [75]. Before the termination condition occurs, the procedure will continue until the ideal software is determined (as indicated in Figure 5). Fitness analysis plays a vital role in MEP for determining the dataset compatibility of emerging mathematical expressions. In order to find the optimal set of chromosomes to reproduce, the fitness function compares the program's actual and anticipated results. Selection, crossover, and mutation are the tools used by MEP to promote fit programs. When the system hits a certain fitness level, generational threshold, or limit of improvement, the algorithm can cease its repetitive procedures and remain in charge. Mutations in MEP are a mechanism by which evolution modifies linear chromosomal components. Minor alterations to the genetic code increase genetic diversity in populations. Mutations, initiated early in the MEP optimization process, alter the genetic material of successive generations, enabling the exploration of diverse solutions. The algorithm's functionality in searching solution spaces and adapting to fitness landscapes is enhanced with the introduction of mutations. The MEP model permits component merger, similar to other ML paradigms. Alphabet or code size, function number crossover frequency, and subpopulation count are crucial factors to think about when doing MEP [76]. Assessing the populace gets increasingly tedious and time-consuming as the number of individuals equals the number of packages. Code length plays a critical role in determining the computational output generated during the process. Keeping in mind the MEP properties mentioned in Table 3 is essential for building a dependable mechanical property model.

When evaluating and modeling using the MEP technique, it is common practice to use datasets that comprise published literature [77,78]. Some researchers suggest that popular linear GP methods, such as MEP, may offer superior performance in predicting the real-world

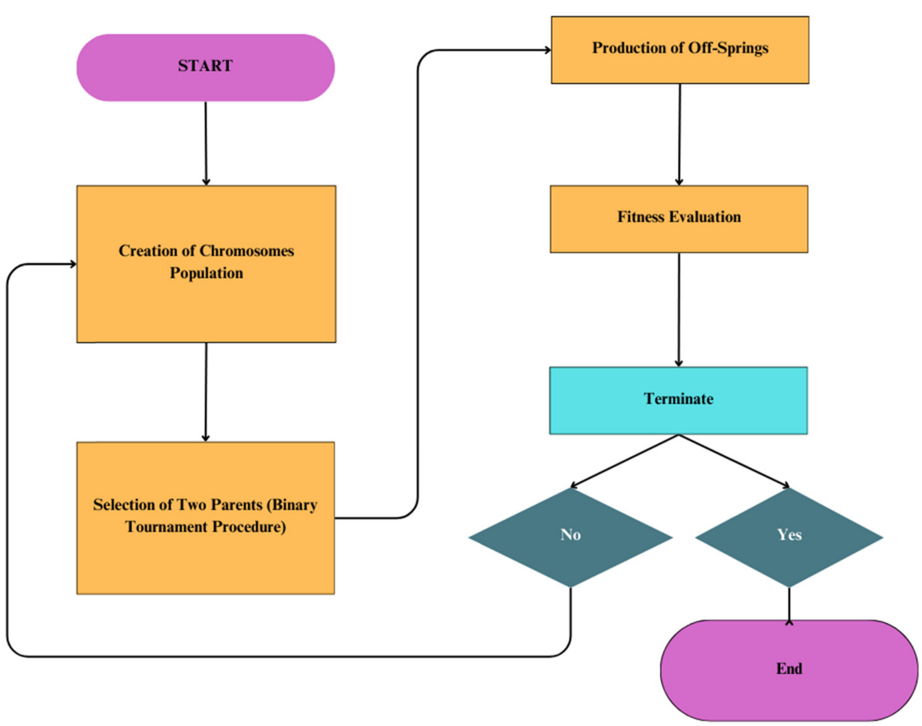

Figure 5: MEP process flow diagram [72].

properties of concrete. For instance, Grosan and Abraham identified an optimal neural network approach by combining linear genomic programming with maximum likelihood estimation [79]. One notable distinction between the two is the operational approach of the GEP, which is undeniably more intricate than that of the MEP [76]. Notwithstanding the reduced density of MEP relative to GEP, significant differences are present between the two: (i) MEP facilitates the reprocessing of code; (ii) encased by chromosomes, non-coding constituents are not obligatory to be exhibited at a precise position; and (iii) it clearly encodes references to function arguments [80]. Due to the structured design of standard GEP genes, with defined "head" and "tail" regions that facilitate the generation of syntactically correct programs, many consider GEP to be a more powerful and capable modeling technique [75]. This finding calls for a more in-depth examination of the limitations and challenges associated with each GP technique.

2.3 Substantiation of models

The models built using GEP and MEP were subjected to statistical analysis using a test set. All of the models' computed metrics consist of root mean square error (RMSE), Pearson's correlation coefficient (r), mean bias error (MBE), Nash–Sutcliffe efficiency (NSE), mean absolute error (MAE), mean absolute percentage error (MAPE), and normalized root mean square error (NRMSE) [57,78,81–83]. The formulas for several statistical indicators are given as

$$r = \frac{\sum_{i=1}^{n}(O_i - \bar{O})(P_i - \bar{P})}{\sqrt{\sum_{i=1}^{n}(O_i - \bar{O})^2}\sqrt{\sum_{i=1}^{n}(P_i - \bar{P})^2}}, \tag{2}$$

$$\text{MAE} = \frac{1}{n}\sum_{i=1}^{n}|O_i - Pi|, \tag{3}$$

$$\text{RMSE} = \sqrt{\sum_{i=1}^{n}\frac{(O_i - P_i)^2}{n}}, \tag{4}$$

$$\text{NRMSE} = \frac{\text{RMSE}}{\bar{O}}, \tag{5}$$

$$\text{MAPE} = \frac{100}{n}\sum_{i=1}^{n}\frac{|O_i - P_i|}{O_i}, \tag{6}$$

$$\text{MBE} = \frac{1}{n}\sum_{i=1}^{n}(P_i - O_i), \tag{7}$$

$$\text{NSE} = 1 - \frac{\sum_{i=1}^{n}(O_i - P_i)^2}{\sum_{i=1}^{n}(O_i - \bar{O})^2}, \tag{8}$$

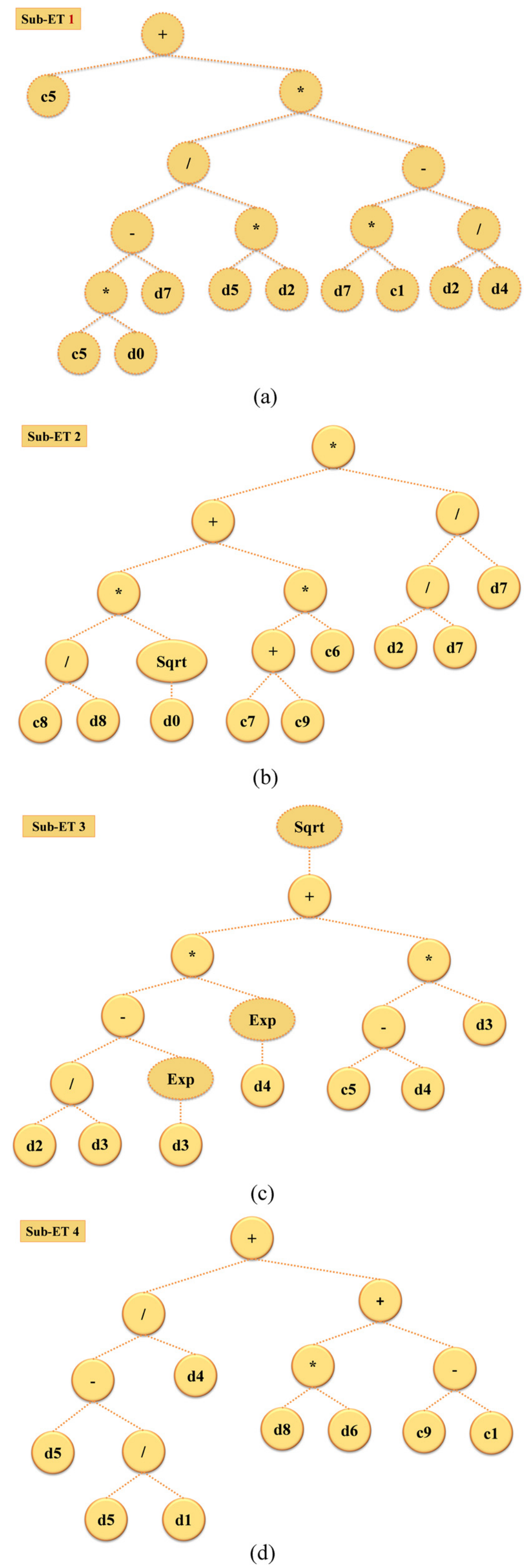

Figure 6: C-S GEP expression tree schematic: (a) Sub-ET 1; (b) Sub-ET 2; (c) Sub-ET 3; (d) Sub-ET 4.

$$a20 - \text{index} = \frac{m20}{M}. \tag{9}$$

In the context of the above equations, O_i represents the observed value, P_i denotes the predicted value, $\bar{O}$ signifies the mean of the observed values, $\bar{P}$ indicates the mean of the predicted values, and n represents the total number of data points.

With M being the dataset size and $m20$ the entry count, this accounts for an expected or experimental value ranging from 0.80 to 1.20, as stated in Eq. (8) [84]. The prediction model indicates that an $a20$-index of 1% would be optimal. This index reflects the performance of the physical engineering approach by measuring the proportion of samples that fall within a 20% uncertainty range of the experimental values. Another key metric for assessing a model's predictive accuracy is the correlation coefficient (r), where higher values of r signify a stronger correlation between predicted and actual outcomes [85]. The value of component R remains unchanged regardless of whether it is divisible or multiplied. Since it takes into account both actual and predicted results, R^2 provide a closer estimate of the true value. R^2 values that are higher and approach 1 indicate a more accurate and robust model construction [86,87]. Like MAE and RMSE, the proposed model shows significant improvements as the number of errors increases, leading to even greater performance with fewer mistakes. The amount of errors grows, but both approaches eventually approach zero [88,89]. Closer inspection, however, showed that MAE truly excels in continuous and smooth databases [90]. In most cases, the model performs better when the previously computed error values are smaller.

Two effective approaches for assessing a model's predictive performance are statistical validation and the use of a Taylor diagram. The Taylor diagram provides a visual means of evaluating the accuracy and reliability of models by comparing their deviations from a reference point or observed data [91,92]. At the actual value point, circular lines represent RSMEs, radial lines show correlation coefficients, and the x- and y-axes display standard deviations. With these three measures, you might be able to locate your model's optimal point. The top model is the most reliable one if we look at its prediction accuracy [91].

3 Results and analysis

3.1 C-S GEP model

Figure 6(a)–(d) present the expression trees (ETs) generated using the GEP technique for the C-S dataset of

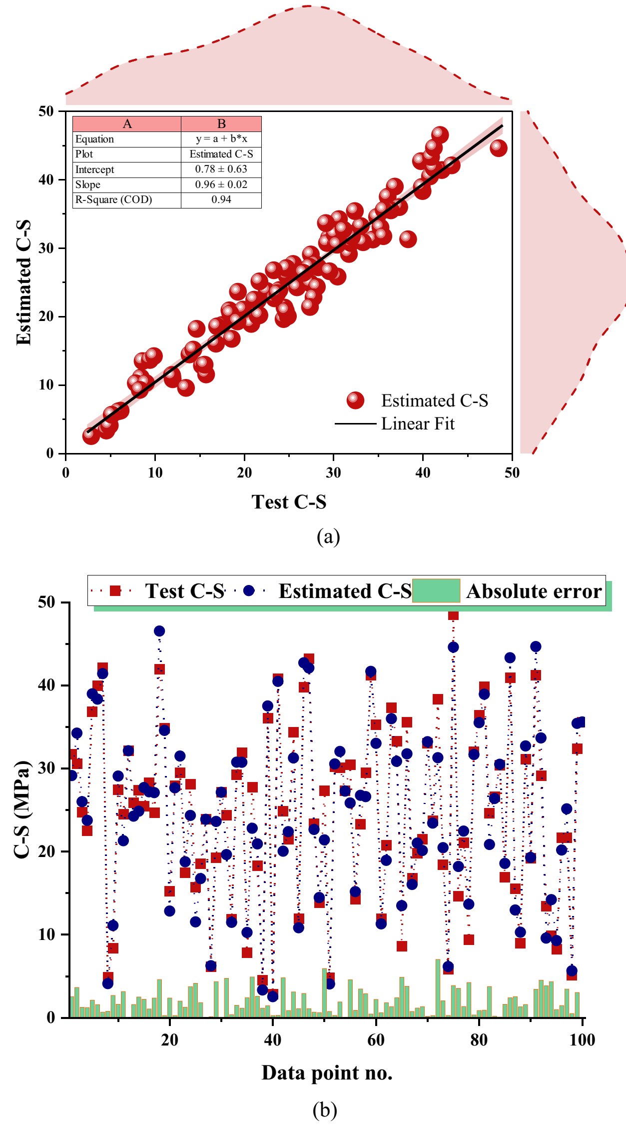

Figure 7: (a) Predicted *vs* test C-S relationships using the GEP model; and (b) error distribution analysis.

foamcrete. These ETs represent the mathematical relationships (Eqs. (10)–(14)) derived from the input parameters to predict the C-S of foamcrete. The ETs, built using a range of mathematical operations like addition, square roots, subtraction, division, multiplication, and exponentiation, play a key role in modeling compressive strength. By encoding these operations, the GEP method generates arithmetic formulas capable of estimating the future C-S based on the input data. These models, when provided with sufficient data, have the potential to outperform idealized models under optimal conditions. Figure 7(a) displays the scatter plot comparing the test and estimated C-S values generated by the GEP model, with the black line representing the perfect fit line. The GEP model exhibited significant

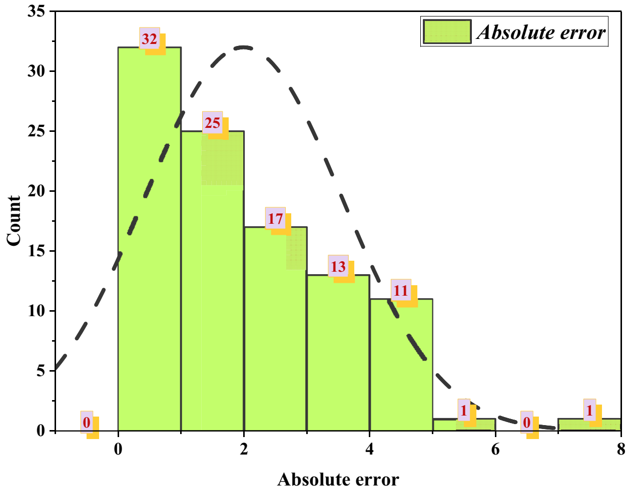

Figure 8: GEP error distribution frequency distribution plot.

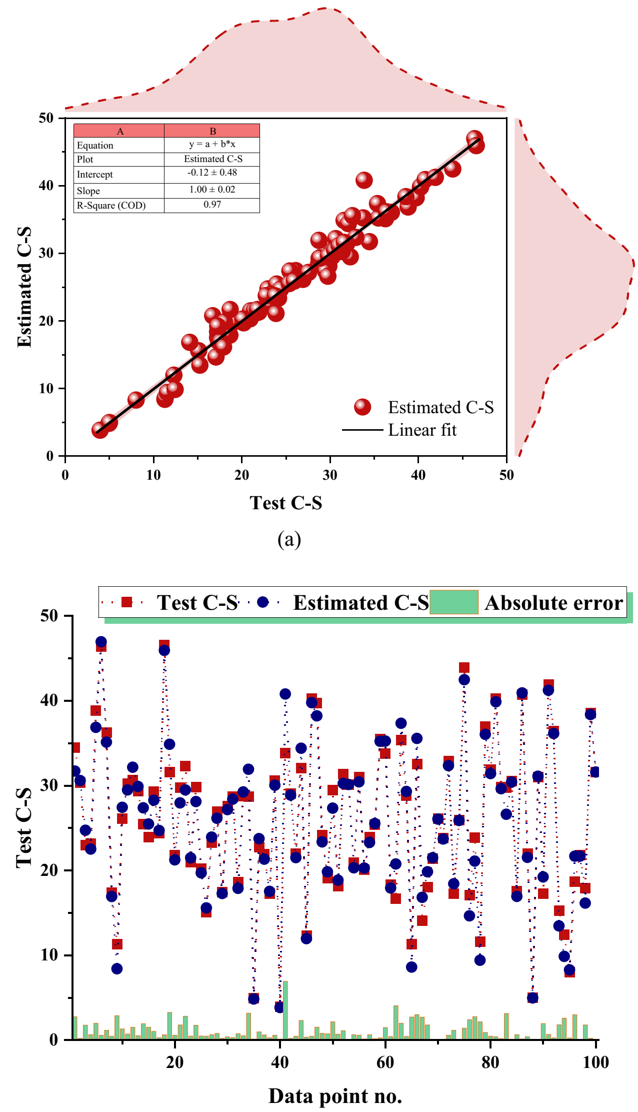

(a)

(b)

Figure 9: (a) Predicted *vs* test C-S relationships using the MEP model and (b) error distribution analysis.

accuracy, evidenced by a high R^2 value of 0.94. The coefficient of determination (R^2) reflects how well the model's predicted values correspond to the actual observed values. In ML models, a greater R^2 value (approaching 1) signifies a superior fit, indicating that the model can account for a substantial percentage of the variance in the output variable, hence validating the model's correctness and reliability.

Figure 7(b) illustrates the error distribution between the test and estimated C-S values across all data points. The plot shows that the estimated C-S values align well with the test results, as depicted by the closeness of the data to the reference line. In terms of the error values, the maximum error recorded is 7.04 MPa, while the minimum is 0.004 MPa, with an average error of 1.99 MPa. The distribution of errors indicates as shown in Figure 8 that 32 data points have errors below 1.0 MPa, 42 points have errors between 1.0 and 3.0 MPa, and 26 points have errors greater than 3.0 MPa. This suggests that the majority of predictions fall within a reasonable acceptable error range for lightweight structural and nonstructural applications, where variations of ±2 MPa are generally considered tolerable [93]. Both the high R^2 value (0.94) and the error distribution further validate the strong prediction capability of the GEP method for the C-S dataset of foamcrete, confirming the model's reliability and accuracy in estimating the compressive strength of foamcrete. This confirms the reliability of the developed models for real-world foamcrete strength prediction

$$\text{C-S(MPa)} = A + B + C + D, \tag{10}$$

$$A = \left(-5.582 + \left(\frac{1.185D_{\mathrm{n}} - F_{\mathrm{m}})}{\mathrm{SS} \times S_{\mathrm{a}}}\right)\left(-2.216F_{\mathrm{m}} + \frac{S_{\mathrm{a}}}{\mathrm{WCR}}\right)\right), \tag{11}$$

$$B = \left(\left(\frac{-13.971 \times \sqrt{D_{\mathrm{n}}}}{A}\right) + (F_{\mathrm{m}} - 13.211)\left(\frac{S_{\mathrm{a}}}{(F_{\mathrm{m}})^2}\right)\right), \tag{12}$$

$$C = \left(\sqrt{\frac{\frac{S_{\mathrm{a}}}{\mathrm{SCR}} - e^{\mathrm{SCR}}}{e^{\mathrm{WCR}}} + (-12.11 - \mathrm{WCR}) \times \mathrm{SCR}}\right), \tag{13}$$

$$D = \left(\frac{A_{\mathrm{g}} - \frac{\mathrm{SS}}{D_{\mathrm{n}}}}{\mathrm{WCR}} + A \times A_{\mathrm{g}} - 8.799\right), \tag{14}$$

where D_{n} is the density, CM is the cement, S_{a} is the sand, SCR is the sand-to-cement ratio, WCR is the water-to-cement ratio, SS is the sand size, A_{g} is the foaming agent,

F_m is the foam content, A is the age, and C-S is the compressive strength.

3.2 CS-MEP model

A practical formula was established to ascertain the C-S of foamcrete, based on the results of the MEP technique and considering the influence of nine independent variables. The concluding set of mathematical equations produced during the modeling procedure is delineated as follows:

$$\text{C-S}\quad(\text{MPa}) = A + B, \tag{15}$$

$$A = \left(\left(\left(\frac{A - \frac{\text{CM}\times\text{SS}}{\text{SCR}(\text{CM}-F_m)^2}}{\log(F_m)} + \frac{|\text{CM}-F_m|\times\sqrt{\text{SCR}}}{\sqrt{\text{WCR}}}\right) + \frac{A - \frac{\text{CM}\times\text{SS}}{\text{SCR}(\text{CM}-F_m)^2}}{\log(F_m)}\right) - \frac{A_g}{\frac{F_m}{\frac{\text{CM}-F_m}{\text{SS}} - \text{CM} - D_n}}\right) - \text{WCR}\right) \tag{16}$$

$$B = \left(\log\left(\frac{\text{CM}\times\text{SS}}{\text{SCR}(\text{CM}-F_m)^2}\right) - \frac{\text{CM}-F_m}{\text{SS}}\right), \tag{17}$$

where D_n is the density, CM is the cement, S_a is the sand, SCR is the sand-to-cement ratio, WCR is the water-to-cement ratio, SS is the sand size, A_g is the foaming agent, F_m is the foam content, A is the age, and C-S is the compressive strength.

Figure 9(a) displays a scatter plot comparing the predicted and actual C-S values based on the MEP model, with the black line representing the line of perfect agreement. The close clustering of data points around this line highlights the excellent predictive accuracy of the MEP model. An R^2 value of 0.97 further confirms its strong performance, indicating that the model explains nearly all the variability in the C-S data. In ML, such a high R^2 and close alignment with the ideal fit line are key indicators of a model's reliability and effectiveness in capturing real-world trends.

Figure 9(b) illustrates the error distribution between the predicted and actual C-S values across all test data points. The plot demonstrates a strong alignment between the estimated and observed values, with most errors clustering near the reference line. The error analysis indicates a maximum deviation of 6.93 MPa, a minimum of 0.01 MPa, and an average error of 1.13 MPa, reflecting the model's high predictive accuracy. Notably, 62 data points exhibit errors below 1.0 MPa, 32 points fall between 1.0 and 3.0 MPa, and only 6 points show errors above 3.0 MPa, as shown in Figure 10. This distribution indicates that the MEP model consistently delivers accurate predictions with minimal deviation falling within the acceptable range of ±2 MPa for lightweight structural and nonstructural applications [93]. Both the high R^2 value of 0.97 and the error distribution validate the MEP method's superior prediction capability for the foamcrete C-S dataset, exceeding the performance of the GEP method. MEP outperforms GEP due to its efficient chromosome structure, where multiple expressions are encoded within a single chromosome, allowing for the selection of the best-performing solution. This approach enhances convergence speed, as multiple candidate solutions are evaluated simultaneously [94]. MEP also shows greater robustness to overfitting by

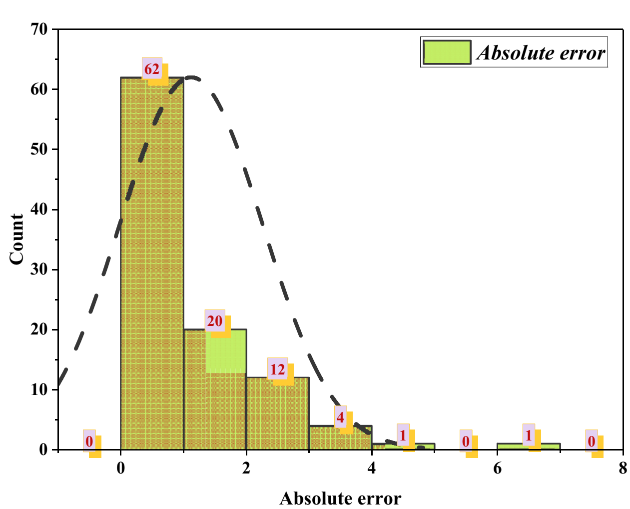

Figure 10: MEP error distribution frequency distribution plot.

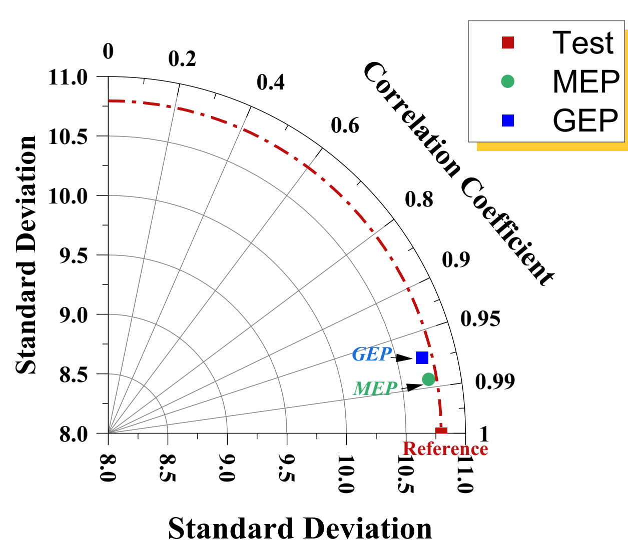

Figure 11: Validating C-S model precision with Taylor's diagram.

Table 4: Results of the statistical analysis

Metrics	C-S	
	GEP	MEP
MAE (MPa)	1.993	1.121
MBE (MPa)	0.100	0.068
RMSE (MPa)	2.533	1.592
NRMSE (MPa)	0.103	0.062
MAPE (%)	10.10	5.00
r	0.972	0.985
NSE	0.944	0.969
a20-index	0.900	0.960

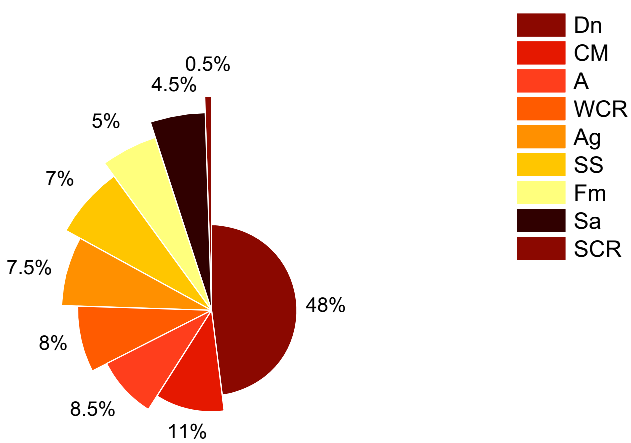

Figure 12: Sensitivity analysis pie chart.

improving generalization across datasets. Its linear representation makes the model more interpretable and easier to analyze compared to the tree-based format of GEP. Additionally, MEP offers better computational efficiency due to its simpler decoding process [95]. These combined advantages explain MEP's superior predictive performance observed in the study.

3.3 Model's validation

R, RMSE, MAE, RRMSE, RSE, NSE, and the results from Eqs. (2)–(9) are summarized in Figure 4, which also includes the outcomes of the efficacy and error evaluations. Reducing error levels often improve the accuracy of model predictions. This is especially true when comparing the C-S MEP model to the C-S GEP model: the former achieves a much lower MAE (from 1.993 to 1.121 MPa) and a far lower MAPE (from 10.10% to 5.00%). Following suit are other error-based measures, such as NRMSE, MBE, and RMSE. With a slightly higher Nash–Sutcliffe efficiency (0.969) than the latter's 0.944, the C-S MEP model achieves better efficiency than the C-S GEP model. Both models produce findings that are similar when we use Pearson's coefficient (*r*). Figure 11 shows the Taylor diagram, which compares all forecasting models. It shows that MEP models are close to one another when predicting the C-S of foamcrete, but GEP models are farther away. The MEP model is the best ML-based method for predicting the C-S of foamcrete because it has the lowest error, highest R^2 value, and the fewest standard deviations, which is consistent with previous research (Table 4).

3.4 Sensitivity analysis

The study examines how input parameters affect foamcrete's C-S prediction. Strong correlation between input factors and anticipated output [96]. Figure 12, which displays how each input impacts the C-S of foamcrete, provides a glimpse into the future of building materials and concrete. The foamcrete density (Dn) is the most important factor, explaining 48% of the variation in C-S predictions. Other factors include cement content (11.0%), age (8.5%), WCR (8.0%), foaming agent (Ag) (7.5%), SS (7.0%), foam content (Fm) (5.0%), sand (Sa) (4.5%), and SCR (0.5%). The outcomes of the sensitivity analysis were significantly influenced by both the number of data points and the number of model parameters. Notably, certain input variables, such as the proportions of concrete mix components, had varying impacts on the results when analyzed using the ML approach. To determine the relative importance of each input parameter within the model, Eqs. (18) and (19) were employed

$$N_i = f_{\max}(x_i) - f_{\min}(x_i), \quad (18)$$

$$S_i = \frac{N_i}{\sum_{j-i}^{n} N_j}, \quad (19)$$

where $f_{\min}(x_i)$ is the lowest projected value through the ith outputs and $f_{\max}(x_i)$ is the maximum.

4 Discussions

There is a limited range of nine input parameters that the GEP and MEP models used in this study can accommodate; hence, the predictions will be particular to foamcrete depending on the dataset provided. The C-S projections will be accurate because each model has the same unit measurements and testing methodology. The models learn the mix's layout and how each parameter influences it using mathematical calculations. The anticipated models will be useless if you use any mix of the nine inputs in the composite analysis. Inconsistent or variable units of the input parameters may result in the models underestimating or overestimating outcomes. Uniform unit dimensions are essential for optimal model performance. Accurate correlation with the training data utilized for these models is also essential. In its absence, they could not function as anticipated. ML models are increasingly applied in the construction sector for tasks such as estimating material strength, ensuring quality control, assessing risks, performing predictive maintenance, and improving energy efficiency. However, several challenges persist. A major concern is the dependency on human input, which can introduce inaccuracies and compromise data reliability. To overcome these limitations, future research should pursue various strategies to enhance ML-based solutions. These may include integrating IoT devices, developing hybrid modeling approaches, leveraging explainable AI techniques, emphasizing sustainability, and customizing data collection and distribution methods to suit specific industry needs. Emerging technical advancements may induce a transformation in the building sector. These technologies can enhance ecological sustainability, mitigate project delays, and improve safety by rendering processes more efficient, intelligible, and transparent, and facilitating informed decision-making. The study's findings may prompt a transition to more environmentally sustainable building practices and an increased use of durable, eco-friendly materials.

5 Conclusions

This study aims to apply ML techniques, specifically GEP and MEP, to predict the C-S of foamcrete, thereby supporting its broader practical implementation. A comprehensive experimental dataset sourced from existing literature was utilized for model development and evaluation. Model validation was performed using multiple assessment tools, including statistical analysis, Taylor diagrams, and the coefficient of determination (R^2). The key findings of the study are summarized below:

- The GEP technique achieved a high prediction accuracy for the C-S of foamcrete, with an R^2 value of 0.94. However, the MEP approach performed even better, attaining a superior R^2 value of 0.970, indicating greater predictive accuracy.
- The mean disparity between predicted and experimental C-S in the GEP approach was 1.99 MPa, compared to 1.13 MPa in the MEP approach. With these error rates, the MEP technique clearly outperformed the GEP model when it came to forecasting the C-S of foamcrete.
- Statistical validation confirms the efficacy of the models, with improvements observed in both the R^2 values and error rates of the ML models. In particular, the MAPE was 11.0% in the GEP model and 5.0% in the MEP model. With RMSE values of 1.592 and 2.533 MPa, respectively, the MEP model fared better than the GEP model. These results provide more evidence that the models' performance is valid in many respects.
- Density had the highest impact on the C-S estimation of foamcrete (48.0% according to the sensitivity study), followed by the cement content at 11.0%, age at 8.5%, WCR at 8.0%, foaming agent at 7.5%, SS at 7.0%, foam content at 5.0%, sand at 4.5%, and SCR at 0.5%.

Their different mathematical approaches are the foundation of GEP and MEP's significance for characteristic prediction in different datasets. These methods provide an efficient way to assess, improve, and optimize the composition of concrete mixtures. The mathematical models developed in this study enable professionals to effectively evaluate and enhance concrete mixtures, promoting swift progress in the discipline.

Acknowledgments: The authors acknowledge their respective institutions/departments for supporting this study.

Funding information: The authors state no funding involved.

Author contributions: G.W.: conceptualization, formal analysis, methodology, data acquisition, supervision, writing-original draft. W.F.: project administration, resources, visualization, validation, writing, reviewing, and editing. Q.S.: data acquisition, conceptualization, software, methodology, writing, reviewing, and editing. Y.L.: software, formal analysis, resources, validation, writing, reviewing, and editing. All authors have accepted responsibility for the entire content of this manuscript and approved its submission.

Conflict of interest: The authors state no conflict of interest.

Data availability statement: The dataset generated and/or analyzed during the current study are available from the corresponding author upon reasonable request.

References

[1] Nambiar, E. K. K. and K. Ramamurthy. Influence of filler type on the properties of foam concrete. *Cement and Concrete Composites*, Vol. 28, 2006, pp. 475–480.

[2] Wang, Y., S. Zhang, D. Niu, L. Su, and D. Luo. Strength and chloride ion distribution brought by aggregate of basalt fiber reinforced coral aggregate concrete. *Construction and Building Materials*, Vol. 234, 2020, id. 117390.

[3] Narayanan, J. S. and K. Ramamurthy. Identification of set-accelerator for enhancing the productivity of foam concrete block manufacture. *Construction and Building Materials*, Vol. 37, 2012, pp. 144–152.

[4] Jones, M. R., K. Ozlutas, and L. Zheng. High-volume, ultra-low-density fly ash foamed concrete. *Magazine of Concrete Research*, Vol. 69, 2017, pp. 1146–1156.

[5] Kilincarslan, Ş., M. Davraz, and M. Akça. The effect of pumice as aggregate on the mechanical and thermal properties of foam concrete. *Arabian Journal of Geosciences*, Vol. 11, 2018, pp. 1–6.

[6] Niu, D., L. Zhang, Q. Fu, B. Wen, and D. Luo. Critical conditions and life prediction of reinforcement corrosion in coral aggregate concrete. *Construction and Building Materials*, Vol. 238, 2020, id. 117685.

[7] Falliano, D., D. De Domenico, G. Ricciardi, and E. Gugliandolo. Experimental investigation on the compressive strength of foamed concrete: Effect of curing conditions, cement type, foaming agent and dry density. *Construction and Building Materials*, Vol. 165, 2018, pp. 735–749.

[8] Liu, T., Y. J. Zhong, Z. L. Han, and W. Xu. Deformation characteristics and countermeasures for a tunnel in difficult geological environment in NW China. *Advances in Civil Engineering*, Vol. 2020, 2020, id. 1694821.

[9] Wei, Y., W. Guo, and Q. Zhang. A model for predicting evaporation from fresh concrete surface during the plastic stage. *Drying Technology*, Vol. 38, 2020, pp. 2231–2241.

[10] Othuman, M. A. and Y. C. Wang. Elevated-temperature thermal properties of lightweight foamed concrete. *Construction and Building Materials*, Vol. 25, 2011, pp. 705–716.

[11] Sayadi, A. A., J. V. Tapia, T. R. Neitzert, and G. C. Clifton. Effects of expanded polystyrene (EPS) particles on fire resistance, thermal conductivity and compressive strength of foamed concrete. *Construction and Building Materials*, Vol. 112, 2016, pp. 716–724.

[12] Tada, S. Material design of aerated concrete—An optimum performance design. *Materials and Structures*, Vol. 19, 1986, pp. 21–26.

[13] Kim, H.-K., J. H. Jeon, and H.-K. Lee. Workability, and mechanical, acoustic and thermal properties of lightweight aggregate concrete with a high volume of entrained air. *Construction and Building Materials*, Vol. 29, 2012, pp. 193–200.

[14] Valore, R. C. Cellular concretes part 2 physical properties. *Journal Proceedings*, Vol. 50, No. 6, 1954, pp. 817–836.

[15] Huang, Z., T. Zhang, and Z. Wen. Proportioning and characterization of Portland cement-based ultra-lightweight foam concretes. *Construction and Building Materials*, Vol. 79, 2015, pp. 390–396.

[16] Decký, M., M. Drusa, K. Zgútová, M. Blaško, M. Hájek, and W. Scherfel. Foam concrete as new material in road constructions. *Procedia Engineering*, Vol. 161, 2016, pp. 428–433.

[17] Kadela, M. and M. Kozłowski. Foamed concrete layer as sub-structure of industrial concrete floor. *Procedia Engineering*, Vol. 161, 2016, pp. 468–476.

[18] Zhang, Z., J. L. Provis, A. Reid, and H. Wang. Mechanical, thermal insulation, thermal resistance and acoustic absorption properties of geopolymer foam concrete. *Cement and Concrete Composites*, Vol. 62, 2015, pp. 97–105.

[19] Zhang, Z. Q. and J. L. Yang. Improving safety of runway overrun through foamed concrete aircraft arresting system: An experimental study. *International Journal of Crashworthiness*, Vol. 20, 2015, pp. 448–463.

[20] Wei, Y., J. Huang, and S. Liang. Measurement and modeling concrete creep considering relative humidity effect. *Mechanics of Time-Dependent Materials*, Vol. 24, 2020, pp. 161–177.

[21] Li, X., C. Qi, and P. Zhang. A micro-macro confined compressive fatigue creep failure model in brittle solids. *International Journal of Fatigue*, Vol. 130, 2020, id. 105278.

[22] Tarasov, A. S., E. P. Kearsley, A. S. Kolomatskiy, and H. F. Mostert. Heat evolution due to cement hydration in foamed concrete. *Magazine of Concrete Research*, Vol. 62, 2010, pp. 895–906.

[23] Favaretto, P., G. E. N. Hidalgo, C. H. Sampaio, R.A. Silva, and R. T. Lermen. Characterization and use of construction and demolition waste from south of Brazil in the production of foamed concrete blocks. *Applied Sciences*, Vol. 7, 2017, id. 1090.

[24] Zhang, Z., J. L. Provis, A. Reid, and H. Wang. Geopolymer foam concrete: An emerging material for sustainable construction. *Construction and Building Materials*, Vol. 56, 2014, pp. 113–127.

[25] Hulimka, J., R. Krzywoń, and A. Jędrzejewska. Laboratory tests of foam concrete slabs reinforced with composite grid. *Procedia Engineering*, Vol. 193, 2017, pp. 337–344.

[26] Wei, S., C. Yiqiang, Z. Yunsheng, and M. R. Jones. Characterization and simulation of microstructure and thermal properties of foamed concrete. *Construction and Building Materials*, Vol. 47, 2013, pp. 1278–1291.

[27] Amran, Y. H. M., N. Farzadnia, and A. A. A. Ali. Properties and applications of foamed concrete; A review. *Construction and Building Materials*, Vol. 101, 2015, pp. 990–1005.

[28] Ramamurthy, K., E. K. K. Nambiar, and G. I. S. Ranjani. A classification of studies on properties of foam concrete. *Cement and Concrete Composites*, Vol. 31, 2009, pp. 388–396.

[29] Zheng, Y., J. Xiong, T. Liu, X. Yue, and J. Qiu. Performance of a deep excavation in Lanzhou strong permeable sandy gravel strata. *Arabian Journal of Geosciences*, Vol. 13, 2020, pp. 1–17.

[30] Sun, H., Q. Wang, P. Zhang, Y. Zhong, and X. Yue. Spatialtemporal characteristics of tunnel traffic accidents in China from 2001 to present. *Advances in Civil Engineering*, Vol. 2019, 2019, id. 4536414.

[31] Wang, L., C. Li, J. Qiu, K. Wang, T. Liu, and H. Li. Treatment and effect of loess metro tunnel under surrounding pressure and water immersion environment. *Geofluids*, Vol. 2020, 2020, id. 7868157.

[32] Wang, X., L. Li, M. Wei, Y. Xiang, Y. Wu, B. Zhou, et al. Experimental study on the mechanical properties of short-cut basalt fiber reinforced concrete under large eccentric compression. *Scientific Reports*, Vol. 15, 2025, id. 10845.

[33] Zhang, W., J. Huang, J. Lin, B. Lin, X. Yang, and Y. Huan. Experimental and numerical investigation of mechanical behavior of segmental joint of shield tunneling strengthened by prestressed CFRP plates. *Structures*, Vol. 70, 2024, id. 107634.

[34] Rong, C., Y. Peng, Q. Shi, and P. Wang. Eccentric compression performance of concrete filled steel tube slotted columns: Experiment and simulation analysis. Structures, Vol. 74, 2025, id. 108580.

[35] Zhang, W., X. Liu, Y. Huang, and M.-N. Tong. Reliability-based analysis of the flexural strength of concrete beams reinforced with

hybrid BFRP and steel rebars. *Archives of Civil and Mechanical Engineering*, Vol. 22, 2022, id. 171.
[36] Fu, Y., X. Wang, L. Wang, and Y. Li. Foam concrete: A state-of-the-art and state-of-the-practice review. *Advances in Materials Science and Engineering*, Vol. 2020, 2020, id. 6153602.
[37] Tikalsky, P. J., J. Pospisil, and W. MacDonald. A method for assessment of the freeze–thaw resistance of preformed foam cellular concrete. *Cement and Concrete Research*, Vol. 34, 2004, pp. 889–893.
[38] Sun, C., Y. Zhu, J. Guo, Y. Zhang, and G. Sun. Effects of foaming agent type on the workability, drying shrinkage, frost resistance and pore distribution of foamed concrete. *Construction and Building Materials*, Vol. 186, 2018, pp. 833–839.
[39] Mindess, S. *Developments in the formulation and reinforcement of concrete*, Woodhead Publishing, Cambridge, United Kingdom, 2019.
[40] Zhao, H., H. Yu, Y. Yuan, and H. Zhu. Blast mitigation effect of the foamed cement-base sacrificial cladding for tunnel structures. *Construction and Building Materials*, Vol. 94, 2015, pp. 710–718.
[41] Choi, H. and S. Ma. An optimal lightweight foamed mortar mix suitable for tunnel drainage carried out using the composite lining method. *Tunnelling and Underground Space Technology*, Vol. 47, 2015, pp. 93–105.
[42] Li, D., Q. Chen, H. Wang, P. Shen, Z. Li, and W. He. Deep learning-based acoustic emission data clustering for crack evaluation of welded joints in field bridges. *Automation in Construction*, Vol. 165, 2024, id. 105540.
[43] Long, X., M.-H. Mao, T.-X. Su, Y.-T. Su, and M.-K. Tian. Machine learning method to predict dynamic compressive response of concrete-like material at high strain rates. *Defence Technology*, Vol. 23, 2023, pp. 100–111.
[44] Ali, R., M. Muayad, A. S. Mohammed, and P. G. Asteris. Analysis and prediction of the effect of Nanosilica on the compressive strength of concrete with different mix proportions and specimen sizes using various numerical approaches. *Structural Concrete*, Vol. 24, 2023, pp. 4161–4184.
[45] Niu, Y., W. Wang, Y. Su, F. Jia, and X. Long. Plastic damage prediction of concrete under compression based on deep learning. *Acta Mechanica*, Vol. 235, 2024, pp. 255–266.
[46] Ahmad, W., V. S. S. C. S. Veeraghantla, and A. Byrne. Advancing sustainable concrete using biochar: Experimental and modelling study for mechanical strength evaluation. *Sustainability*, Vol. 17, 2025, id. 2516.
[47] Marani, A., A. Jamali, and M. L. Nehdi. Predicting ultra-high-performance concrete compressive strength using tabular generative adversarial networks. *Materials*, Vol. 13, 2020, id. 4757.
[48] Marani, A. and M. L. Nehdi. Machine learning prediction of compressive strength for phase change materials integrated cementitious composites. *Construction and Building Materials*, Vol. 265, 2020, id. 120286.
[49] Nunez, I., A. Marani, and M. L. Nehdi. Mixture optimization of recycled aggregate concrete using hybrid machine learning model. *Materials*, Vol. 13, 2020, id. 4331.
[50] Zhang, J., Y. Huang, F. Aslani, G. Ma, and B. Nener. A hybrid intelligent system for designing optimal proportions of recycled aggregate concrete. *Journal of Cleaner Production*, Vol. 273, 2020, id. 122922.
[51] Zhang, J., D. Li, and Y. Wang. Toward intelligent construction: Prediction of mechanical properties of manufactured-sand concrete using tree-based models. *Journal of Cleaner Production*, Vol. 258, 2020, id. 120665.
[52] Rajasekar, A., K. Arunachalam, and M. Kottaisamy. Assessment of strength and durability characteristics of copper slag incorporated ultra high strength concrete. *Journal of Cleaner Production*, Vol. 208, 2019, pp. 402–414.
[53] Naseri, H., H. Jahanbakhsh, P. Hosseini, and F. M. Nejad. Designing sustainable concrete mixture by developing a new machine learning technique. *Journal of Cleaner Production*, Vol. 258, 2020, id. 120578.
[54] Young, B. A., A. Hall, L. Pilon, P. Gupta, and G. Sant. Can the compressive strength of concrete be estimated from knowledge of the mixture proportions?: New insights from statistical analysis and machine learning methods. *Cement and Concrete Research*, Vol. 115, 2019, pp. 379–388.
[55] Nguyen, N.-H., T. P. Vo, S. Lee, and P. G. Asteris. Heuristic algorithm-based semi-empirical formulas for estimating the compressive strength of the normal and high performance concrete. *Construction and Building Materials*, Vol. 304, 2021, id. 124467.
[56] Abd, A. M. and S. M. Abd. Modelling the strength of lightweight foamed concrete using support vector machine (SVM). *Case Studies in Construction Materials*, Vol. 6, 2017, pp. 8–15.
[57] Iqbal, M. F., Q.-f Liu, I. Azim, X. Zhu, J. Yang, M. F. Javed, et al. Prediction of mechanical properties of green concrete incorporating waste foundry sand based on gene expression programming. *Journal of Hazardous Materials*, Vol. 384, 2020, id. 121322.
[58] Dao, D. V., H. Adeli, H.-B. Ly, L. M. Le, V. M. Le, T.-T. Le, et al. A sensitivity and robustness analysis of GPR and ANN for high-performance concrete compressive strength prediction using a Monte Carlo simulation. *Sustainability*, Vol. 12, 2020, id. 830.
[59] Gandomi, A. H. and A. H. Alavi. A new multi-gene genetic programming approach to nonlinear system modeling. Part I: Materials and structural engineering problems. *Neural Computing and Applications*, Vol. 21, 2012, pp. 171–187.
[60] Taffese, W. Z. and L. Espinosa-Leal. A machine learning method for predicting the chloride migration coefficient of concrete. *Construction and Building Materials*, Vol. 348, 2022, id. 128566.
[61] Ahmed, H. U., A. A. Mohammed, and A. Mohammed. Soft computing models to predict the compressive strength of GGBS/FA-geopolymer concrete. *PloS one*, Vol. 17, 2022, id. e0265846.
[62] Ahmed, H. U., A. S. Mohammed, and A. A. Mohammed. Multivariable models including artificial neural network and M5P-tree to forecast the stress at the failure of alkali-activated concrete at ambient curing condition and various mixture proportions. *Neural Computing and Applications*, Vol. 34, 2022, pp. 17853–17876.
[63] Amin, M. N., R.-U.-D. Nassar, M. T. Qadir, A. Ahmad, K. Khan, and M. F. Javed. Investigating the compressive property of foamcrete and analyzing the feature interaction using modeling approaches. *Results in Engineering*, Vol. 24, 2024, id. 103305.
[64] Lee, B. C. and D. M. Brooks. Accurate and efficient regression modeling for microarchitectural performance and power prediction. *ACM SIGOPS Operating Systems Review*, Vol. 40, 2006, pp. 185–194.
[65] Holland, J. H. *Adaptation in natural and artificial systems: An introductory analysis with applications to biology, control, and artificial intelligence*, MIT Press, Cambridge, United Kingdom, 1992.
[66] Koza, J. On the programming of computers by means of natural selection. *Genetic Programming*, The MIT Press, Cambridge, UK,1992.
[67] Gholampour, A., T. Ozbakkaloglu, and R. Hassanli. Behavior of rubberized concrete under active confinement. *Construction and Building Materials*, Vol. 138, 2017, pp. 372–382.

[68] Topcu, I. B. and M. Sarıdemir. Prediction of compressive strength of concrete containing fly ash using artificial neural networks and fuzzy logic. *Computational Materials Science*, Vol. 41, 2008, pp. 305–311.
[69] Ferreira, C. *Gene expression programming: Mathematical modeling by an artificial intelligence*, Vol 21, Springer, Berlin, Germany, 2006.
[70] Gandomi, A. H., G. J. Yun, and A. H. Alavi. An evolutionary approach for modeling of shear strength of RC deep beams. *Materials and Structures*, Vol. 46, 2013, pp. 2109–2119.
[71] Gandomi, A. H., S. K. Babanajad, A. H. Alavi, and Y. Farnam. Novel approach to strength modeling of concrete under triaxial compression. *Journal of Materials in Civil Engineering*, Vol. 24, 2012, pp. 1132–1143.
[72] Amin, M. N., S. U. Arifeen, M. T. Qadir, F. Alsharari, and M. I. Faraz. AI-powered interpretable models for the abrasion resistance of steel fiber-reinforced concrete in hydraulic conditions. *Case Studies in Construction Materials*, Vol. 22, 2025, id. e04755.
[73] Wang, H.-L. and Z.-Y. Yin. High performance prediction of soil compaction parameters using multi expression programming. *Engineering Geology*, Vol. 276, 2020, id. 105758.
[74] Iqbal, M. F., M. F. Javed, M. Rauf, I. Azim, M. Ashraf, J. Yang, et al. Sustainable utilization of foundry waste: Forecasting mechanical properties of foundry sand based concrete using multi-expression programming. *Science of the Total Environment*, Vol. 780, 2021, id. 146524.
[75] Oltean, M. and C. Grosan. A comparison of several linear genetic programming techniques. *Complex Systems*, Vol. 14, 2003, pp. 285–314.
[76] Fallahpour, A., E. U. Olugu, and S. N. Musa. A hybrid model for supplier selection: integration of AHP and multi expression programming (MEP). *Neural Computing and Applications*, Vol. 28, 2017, pp. 499–504.
[77] Alavi, A. H., A. H. Gandomi, M. G. Sahab, and M. Gandomi. Multi expression programming: A new approach to formulation of soil classification. *Engineering with Computers*, Vol. 26, 2010, pp. 111–118.
[78] Mohammadzadeh, S. D., S.-F. Kazemi, A. Mosavi, E. Nasseralshariati, and J. H. M. Tah. Prediction of compression index of fine-grained soils using a gene expression programming model. *Infrastructures*, Vol. 4, 2019, id. 26.
[79] Grosan, C. and A. Abraham. Stock market modeling using genetic programming ensembles. *In* Genetic systems programming: Theory and experiences, Springer, Berlin, Germany, 2006, 131–146.
[80] Oltean, M. and D. Dumitrescu. Multi expression programming. *Journal of Genetic Programming and Evolvable Machines*, 2002, 1–27.
[81] Shahin, M. A. Genetic programming for modelling of geotechnical engineering systems, In: *Handbook of Genetic Programming Applications*, Springer, Cham, Switzerland, 2015, pp. 37–57.
[82] Çanakcı, H., A. Baykasoğlu, and H. Güllü. Prediction of compressive and tensile strength of Gaziantep basalts via neural networks and gene expression programming. *Neural Computing and Applications*, Vol. 18, 2009, pp. 1031–1041.
[83] Alade, I. O., M. A. Abd Rahman, and T. A. Saleh. Predicting the specific heat capacity of alumina/ethylene glycol nanofluids using support vector regression model optimized with Bayesian algorithm. *Solar Energy*, Vol. 183, 2019, pp. 74–82.
[84] Asteris, P. G., M. Koopialipoor, D. J. Armaghani, E. A. Kotsonis, and P. B. Lourenço. Prediction of cement-based mortars compressive strength using machine learning techniques. *Neural Computing and Applications*, Vol. 33, 2021, pp. 13089–13121.
[85] Alade, I. O., A. Bagudu, T. A. Oyehan, M. A. Abd Rahman, T. A. Saleh, and S. O. Olatunji. Estimating the refractive index of oxygenated and deoxygenated hemoglobin using genetic algorithm–support vector regression model. *Computer Methods and Programs in Biomedicine*, Vol. 163, 2018, pp. 135–142.
[86] Zhang, W., R. Zhang, C. Wu, A. T. C. Goh, S. Lacasse, Z. Liu, et al. State-of-the-art review of soft computing applications in underground excavations. *Geoscience Frontiers*, Vol. 11, 2020, pp. 1095–1106.
[87] Alavi, A. H., A. H. Gandomi, H. C. Nejad, A. Mollahasani, and A. Rashed. Design equations for prediction of pressuremeter soil deformation moduli utilizing expression programming systems. *Neural Computing and Applications*, Vol. 23, 2013, pp. 1771–1786.
[88] Kisi, O., J. Shiri, and M. Tombul. Modeling rainfall-runoff process using soft computing techniques. *Computers & Geosciences*, Vol. 51, 2013, pp. 108–117.
[89] Alade, I. O., M. A. Abd Rahman, and T. A. Saleh. Modeling and prediction of the specific heat capacity of $Al_2 O_3$/water nanofluids using hybrid genetic algorithm/support vector regression model. *Nano-Structures & Nano-Objects*, Vol. 17, 2019, pp. 103–111.
[90] Shahin, M. A. Use of evolutionary computing for modelling some complex problems in geotechnical engineering. *Geomechanics and Geoengineering*, Vol. 10, 2015, pp. 109–125.
[91] Band, S. S., E. Heggy, S. M. Bateni, H. Karami, M. Rabiee, S. Samadianfard, et al. Groundwater level prediction in arid areas using wavelet analysis and Gaussian process regression. *Engineering Applications of Computational Fluid Mechanics*, Vol. 15, 2021, pp. 1147–1158.
[92] Taylor, K. E. Summarizing multiple aspects of model performance in a single diagram. *Journal of Geophysical Research: Atmospheres*, Vol. 106, 2001, pp. 7183–7192.
[93] Faleschini, F., M. A. Zanini, and C. Demartino. Design guidelines for structural and non-structural applications. *In* Handbook of sustainable concrete and industrial waste management, Elsevier, Cambridge, United Kingdom, 2022, pp. 359–386.
[94] Jin, C., Y. Qian, S. A. Khan, W. Ahmad, F. Althoey, B. S. Alotaibi, et al. Investigating the feasibility of genetic algorithms in predicting the properties of eco-friendly alkali-based concrete. *Construction and Building Materials*, Vol. 409, 2023, id. 134101.
[95] Liu, H., S. A. Khan, M. N. Amin, F. Althoey, and M. T. Qadir. Evaluating the strength loss and the effectiveness of glass and eggshell powder for cement mortar under acidic conditions. *Reviews on Advanced Materials Science*, Vol. 63, 2024, id. 20240042.
[96] Ahmad, A., K. A. Ostrowski, M. Maślak, F. Farooq, I. Mehmood, and A. Nafees. Comparative study of supervised machine learning algorithms for predicting the compressive strength of concrete at high temperature. *Materials*, Vol. 14, 2021, id. 4222.